DOI 10.1007/s10593-018-2246-6

Chemistry of Heterocyclic Compounds **2018**, *54*(2), 146–152

New selective "on-off" fluorescence chemosensor based on carbazole Schiff base for Fe^{3+} detection

Yi He[1]*, Jun Yin[2], Guang Wang[2]

[1] *College of Chemistry, Jilin University,*
Changchun 130025, P. R. China; e-mail: heyi@jlu.edu.cn

[2] *Faculty of Chemistry, Northeast Normal University,*
Changchun 130024, P. R. China; e-mail: yinj623@nenu.edu.cn

Published in Khimiya Geterotsiklicheskikh Soedinenii,
2018, *54*(2), 146–152

Submitted November 30, 2017
Accepted January 14, 2018

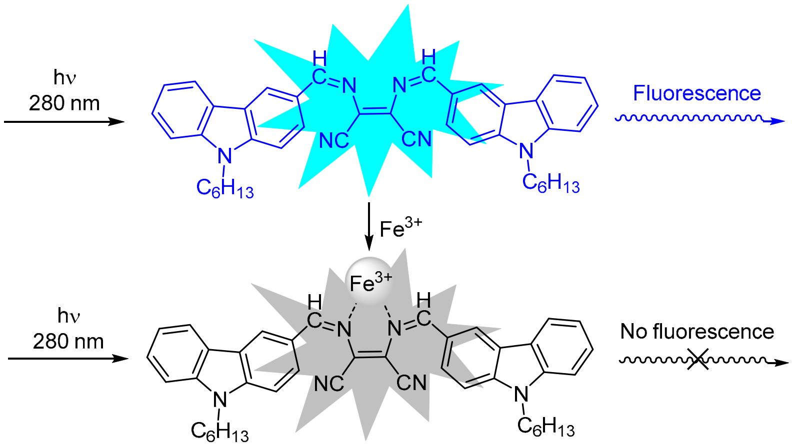

A new double Schiff base, carbazole, and diaminomaleonitrile-based chemosensor for Fe^{3+} with high sensitivity and selectivity was designed and synthesized. Addition of only Fe^{3+} ions induced the fluorescence quenching of the chemosensor in DMF solution. The chemosensor formed a 1:1 complex with Fe^{3+} with the high binding constant of $7.98 \cdot 10^{-6}$ M^{-1}. The chemosensor displayed low detection limit ($3.75 \cdot 10^{-8}$ M) and fast response time (15 s) to Fe^{3+}.

Keywords: carbazole, iron ion, Schiff base, fluorescence chemosensor.

Metal ions play an important role in environment and biology.[1] The excessive ingestion and deposition of heavy transition metal ions in living body is harmful to organism even if the ion is an essential trace metal ion to sustain normal human health.[2–4] In particular, Fe^{3+} plays a very prominent role in biological systems and performs a major function in cells of all organism systems, such as cellular metabolism and transport of oxygen through heme.[5] Also, an interesting paradox is connected with Fe^{3+}, as both its deficiency and excess cause biological disorders in the living body, such as anemia, damage of vital organs, heart failure, and diabetes.[6,7] Therefore, the development of sensitive and accurate methods for determination of the presence, concentration, and location of Fe^{3+} still is extremely important for human health.

Among the methods of detecting metal ions, fluorescent and colorimetric chemosensors have attracted widespread interest of researchers due to high selectivity, high sensitivity, convenient operation, and low cost.[8–12] One of the popular strategies in fluorescent chemosensor design is to combine a fluorophore and an ionophore in one molecule *via* a spacer, while the ionophore containing oxygen, nitrogen, or sulfur atoms can selectively coordinate with metal ions. The optical and optoelectronic properties of the fluorophore are easily influenced by the coordination reaction of ionophore with metal ions. Macroscopically, the fluorescence intensity and color of chemosensor in solution or solid state displays obvious changes.

Many chemosensors for the Fe^{3+} detection with high selectivity and sensitivity have been developed in the resent years. Nanoparticles, polymer dots, and organic fluorophores, such as oxadiazole and coumarin, can be used as fluorophores in Fe^{3+} chemosensors.[13–16] On the other side, the employed coordination units are more diverse.

Carbazole moiety is often used as a core structure in optical and electronic materials. Carbazole derivatives are

Scheme 1

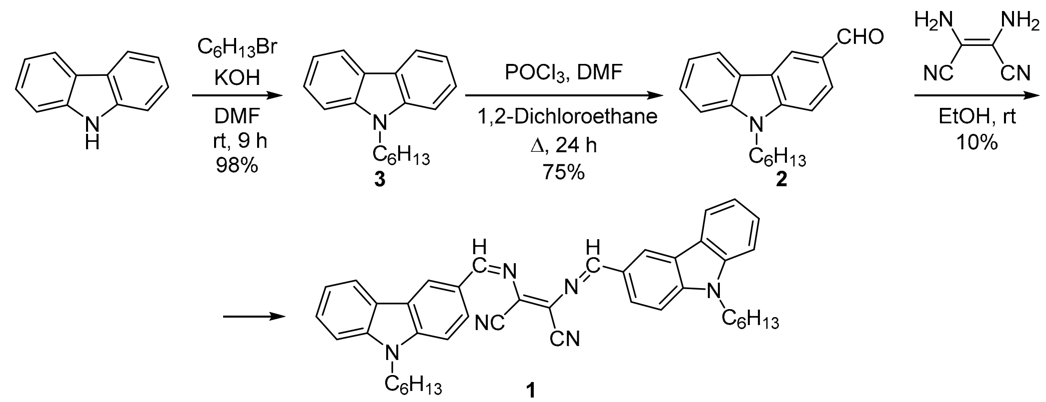

used as photoelectric functional materials, and there are a few reports on carbazole-based fluorescent chemosensors for selective detection of metal ions.[17–19]

Schiff bases, condensation products of reactive aldehydes and amines, are important compounds with various potential applications. Schiff bases attract much interest both from a synthetic and biological points of view. Schiff base derivatives can be used as ionophores in fluorescent chemosensors.[20–23] Diaminomaleonitrile can form Schiff base with an aldehyde group and provide four coordination nitrogen atoms. So the diaminomaleonitrile-based Schiff base would provide special coordination geometry for metal ion.

In this paper, a new chemosensor containing dimeric Schiff base composed of carbazole and diaminomaleonitrile is reported (Scheme 1). This dimeric Schiff base demonstrates the application potential as a fluorescent sensor for the detection of Fe^{3+} with high selectivity and sensitivity in DMF solution.

The general synthetic procedure is given in Scheme 1. The target sensor **1** was easily synthesized in the reaction of 2,3-diaminomaleonitrile with 9-hexyl-9*H*-carbazole-3-carbaldehyde (**2**). The yield was very low (not exceeding 10%) even when 3 equivalents of compound **2** were taken. 9-Hexyl-9*H*-carbazole-3-carbaldehyde (**2**) was synthesized from 9-hexyl-9*H*-carbazole (**3**) with 75% yield, which was obtained with quantitative yield by alkylating 9*H*-carbazole with 1-bromohexane. The alkyl group on the N atom of carbazole core is aimed to increase the solubility of the final product **1** in organic solvents. The structure of sensor **1** was well characterized by IR, ^1H, ^{13}C NMR, and HRMS methods.

The fluorescent emission band of sensor **1** appeared in the range of 330–520 nm with two peaks at 356 nm and 372 nm under the excitation of 280 nm light (Fig. 1). Comparison with the fluorescence spectrum of compound **2** reveals that these emission bands of sensor **1** overlapped with that of compound **2**, for compound **1**, however, another emission band between 380–420 nm appeared. This new emission band should originate from the whole conjugation system of sensor **1**. There are four nitrogen atoms with lone electron pairs in sensor **1**, which coordinate with metal ions and further change the fluorescent property of sensor **1**.

The fluorescence spectra studies revealed that sensor **1** exhibited a high selectivity to Fe^{3+} in DMF solution. Figure 1 presents the fluorescence changes of sensor **1** in DMF ($1 \cdot 10^{-5}$ M) after the addition of different metal ions (10 equiv). Only the addition of Fe^{3+} induced significant fluorescence quenching. On the contrary, addition of 10 equiv of various metal ions, such as K^+, Ag^+, Mn^{2+}, Co^{2+}, Ni^{2+}, Zn^{2+}, Cd^{2+}, Pb^{2+}, Mg^{2+}, Ca^{2+}, Sr^{2+}, Ba^{2+}, Hg^{2+}, Fe^{2+}, Cu^{2+}, Al^{3+}, and Cr^{3+} under the identical conditions did not significantly influence the emission intensity of sensor **1**. Upon addition of 10 equiv Fe^{3+} to sensor **1** solution, a fluorescence quenching up to 60% was observed without an obvious visual change in the color. The quantum yields of sensor **1** in DMF ($1 \cdot 10^{-5}$ M) decreased from 0.13 to 0.09. The fluorescence images of sensor **1** before and after addition of Fe^{3+} in Figure 1 also illustrates the obvious fluorescence quenching after addition of Fe^{3+}. These results indicate that sensor **1** has high selectivity of fluorescence response to Fe^{3+} and could be used as fluorescent chemosensor for selective detection of iron(III) ions.

The fluorescence emission of sensor **1** is strong due to the combination of two carbazole molecules on both ends of diaminomaleonitrile, which constitutes a highly conjugated unit. Additionally, the formation of large conjugated system inhibited C=N isomerization which is the predominant decay process of the excited state.[24] The fluorescence quenching of sensor **1** upon the addition of Fe^{3+} can be attributed to the formation of complex between sensor **1** and Fe^{3+}. Sensor **1** is an electronically conjugated form of two subunits, carbazole (signaling unit) and Schiff base (binding unit). Sensor **1** presented the structural characteristic of charge transfer-type (CT) molecule and its

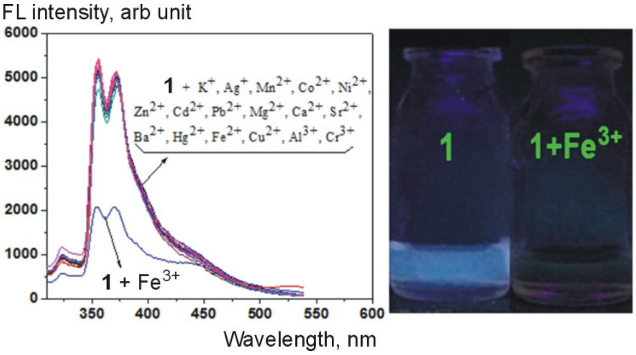

Figure 1. The fluorescence changes of sensor **1** in DMF upon the addition of different metal ions and fluorescence images.

photophysical properties are sensitive to the change of the environment and interacting molecules.[25,26] The binding interaction between sensor **1** and Fe^{3+} *via* the two nitrogen atoms of Schiff base induced the ICT (internal charge transfer) from the electron-rich nitrogen atom of the carbazole moiety to Fe^{3+}-coordinating unit.[27–29] This ligand-to-metal charge transfer (LMCT) is responsible for the fluorescence quenching.[30] On the contrary, other ions failed to form complexes with sensor **1** and did not decrease the fluorescence intensity, this may be explained by the different coordination geometry of sensor **1**, the inappropriate ion radius, or insufficient binding energy of these metal ions.

The anti-jamming ability is also important for the practical applicability of the sensor and selectivity elevating of a specific indicator. The possible interferences with metal ions including K^+, Ag^+, Mn^{2+}, Co^{2+}, Ni^{2+}, Zn^{2+}, Cd^{2+}, Pb^{2+}, Mg^{2+}, Ca^{2+}, Sr^{2+}, Ba^{2+}, Hg^{2+}, Fe^{2+}, Cu^{2+}, Al^{3+}, and Cr^{3+} were measured through competitive experiments. The competition experiment was carried out by monitoring the change of fluorescence intensity of sensor **1** ($1\cdot10^{-5}$ M) at 372 nm upon addition of 10 equiv Fe^{3+} and 10 equiv of the other metal, the results are shown in Figure 2. The addition of above-mentioned competitive metal ion (10 equiv) to the solution of sensor **1** just caused a negligible decrease of fluorescence intensity (Fig. 1). But after further addition of the same concentration of Fe^{3+}, the fluorescence decreased significantly to the same degree as that caused by Fe^{3+} alone (Fig. 2*a*). The fluorescence images also demonstrate high selectivity of sensor **1** for Fe^{3+} (Fig. 2*b*); the fluorescence of sensor **1** disappeared completely after addition of 10 equiv Fe^{3+}. The interaction of the above ions with the sensor in comparison with iron has its own peculiarities. In particular, Cd^{2+} and Ag^+ decreased the fluorescence quenching efficiency of Fe^{3+} on sensor **1**, but the fluorescence intensities of sensor **1** were still quenched over half. On the contrary, Hg^{2+} and Cu^{2+} increased the fluorescence quenching efficiency, which indicated that there are some weak interactions between sensor **1** and Hg^{2+} or Cu^{2+}. However, only these metal ions, without Fe^{3+} ions, could not cause a large change in fluorescence of sensor **1**, which indicated that the fluorescence quenching was almost entirely caused by Fe^{3+}. These results indicate that the existence of the competitive metal ion could not interfere recognition of sensor **1** by Fe^{3+}, in other words, the sensing of sensor **1** toward Fe^{3+} is highly selective. Therefore, it is safe to say that sensor **1** is capable for fluorescent recognition of Fe^{3+} with high selectivity from the above interference metal ions.

Job's plot analysis was used to determine the stoichiometry of sensor **1** and Fe^{3+}. The Job's plot was drawn by plotting $F - (1 - x)F_0$ as a function of x, herein, F is the fluorescence intensity at 372 nm, x is the mole fraction of Fe^{3+}.[31,32] As shown in Figure 3*a*, the plot presents a turning point when the molar fraction of Fe^{3+}/(sensor **1** + Fe^{3+}) was about 0.5, which indicated that the complex stoichiometry of Fe^{3+} and sensor **1** is 1:1. Meanwhile, this conclusion would be proved by Benesi–Hildebrand plot.

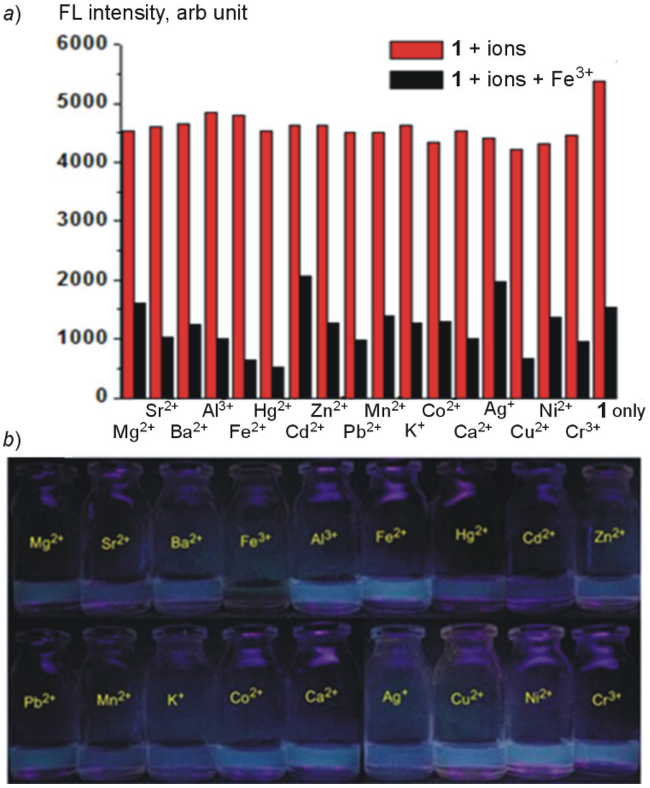

Figure 2. *a*) The fluorescence intensity changes of sensor **1** ($1\cdot10^{-5}$ M) in DMF by various metal ions. The red bars represent the fluorescence intensity of sensor **1** in the presence of miscellaneous metal ions (10 equiv), the black bars represent the fluorescence intensity of the above solution upon further addition of 10 equiv of Fe^{3+} (λ_{em} 372 nm). *b*) Fluorescence images of sensor **1** after addition of different metal ions. (For interpretation of the color in this figure, the reader is referred to the web version of this article.)

Fluorescence titration is often used to evaluate the sensing property of chemosensor toward metal ion. The fluorescence titration experiment of sensor **1** ($1\cdot10^{-5}$ M) with Fe^{3+} (0–20 equiv) in DMF solution was carried out. As shown in Figure 3*b*, upon gradual increase of Fe^{3+} amount, the fluorescence intensity of the solution at 372 nm decreases gradually. The fluorescence intensity reached its lowest value and the quenching efficiency reached 85% ($I_0 - I_{20}/I_0$) when the 20 equiv Fe^{3+} was added. I_0 was the original fluorescence intensity and I_{20} was the fluorescence intensity after adding 20 equiv of Fe^{3+}.

The association constant (K) of sensor **1** with Fe^{3+} is usually calculated using the Benesi–Hildebrand plot. According to the result of Job' plot, the 1:1 binding mode was used in Benesi–Hildebrand plot[33,34] as the following:

$$1/(F_0 - F) = 1/\{K_a(F_0 - F_{min})C\} + 1/(F_0 - F_{min}).$$

Herein, F_0 and F are the fluorescence intensities at 372 nm in the absence and presence of Fe^{3+} ions, respectively. The association constant (K_a) was evaluated graphically by plotting $1/(F_0 - F)$ against $1/Fe^{3+}$ (Fig. 4*a*). Linear fitting of the experiment plot based on the 1:1 binding stoichiometry of sensor **1** and Fe^{3+} was executed and the fitted curve is almost superimposed over the experimental plot with a correlation coefficient over 0.9918, which strongly supports the 1:1 binding stoichiometry of sensor **1** with Fe^{3+}. The binding constant between sensor **1** and Fe^{3+} was evaluated to be $7.98\cdot10^{-6}$ M^{-1}.

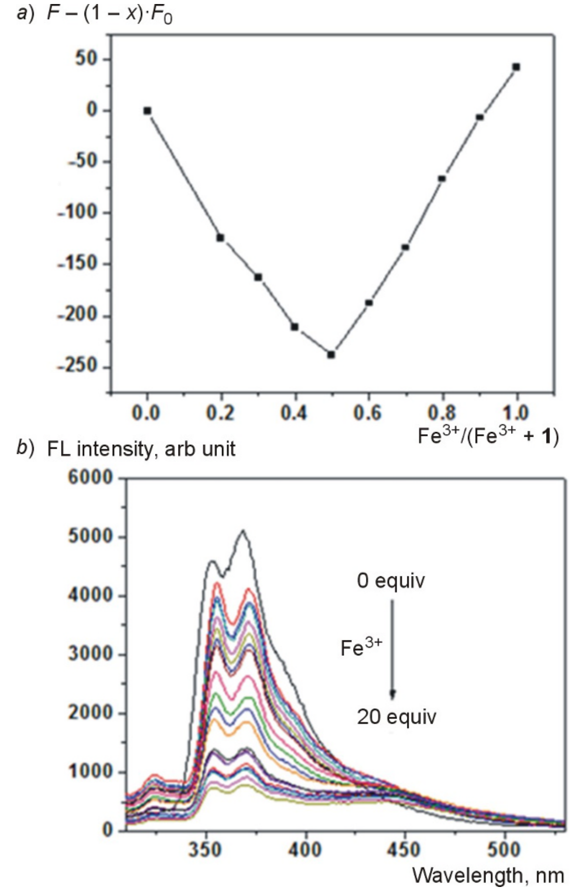

Figure 3. *a*) Job's plot performed using the fluorescence emission spectroscopy of sensor **1** and Fe^{3+} in DMF solution with the total concentration of $5 \cdot 10^{-5}$ M. λ_{ex} 280 nm, λ_{em} 372 nm. *b*) Fluorescence response of sensor **1** in DMF solution ($1 \cdot 10^{-5}$ M) upon addition of Fe^{3+} (0–20 equiv).

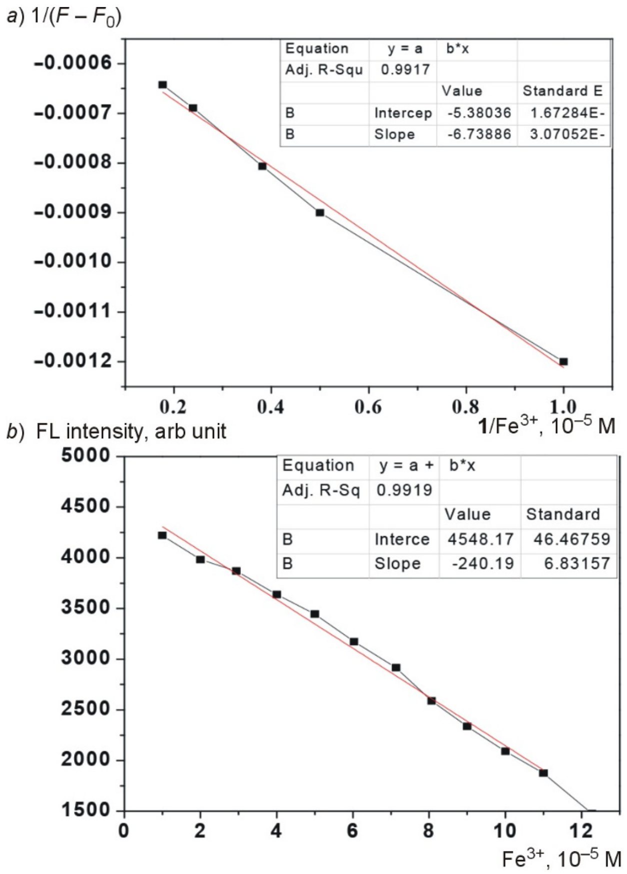

Figure 4. *a*) Benesi–Hildebrand plot of sensor **1** ($1 \cdot 10^{-5}$) in DMF solution in the presence of Fe^{3+} (1.0–5.0 equiv). *b*) The fluorescent calibration curve of sensor **1** ($1 \cdot 10^{-5}$) with different concentrations of Fe^{3+} in DMF (λ_{ex} 280 nm, λ_{em} 372 nm).

The fluorescence quenching detection limit (C_{LOD}) of sensor **1** for Fe^{3+} was further calculated based on the fluorescence titration curve (Fig. 4*b*) and the equation: $C_{LOD} = K \cdot Sb1/S$.

Here, $K = 3$; $Sb1$ is the standard deviation of the blank solution; S is the slope of the calibration curve.[35] As shown in Figure 4*b*, the Fe^{3+} concentration changed over the range of $1 \cdot 10^{-5}$ – $11 \cdot 10^{-5}$ M. A good linear regression equation was reobtained with a correlation coefficient over 0.9920. The detection limit of Fe^{3+} was calculated to be $3.75 \cdot 10^{-8}$ M. Compared with some recent reports,[36] the detection limit of sensor **1** for Fe^{3+} shows a higher sensitivity for Fe^{3+}. In addition, the detection limit is much lower than the limit of Fe^{3+} in drinking water (5.357 μM) permitted by US Environmental Protection Agency (EPA).[37] This result indicates that sensor **1** is sensitive enough to monitor Fe^{3+} concentration in aqueous samples.

Fast response of sensor to metal ions facilitates monitoring of metal ions in real time. The fluorescence intensity of sensor **1** in DMF solution ($1 \cdot 10^{-5}$ M) at 372 nm after addition of Fe^{3+} decreased rapidly to the lowest value within 15 s, which indicates that sensor **1** can form complex with Fe^{3+} and has fast fluorescence response to Fe^{3+} in very short time. So, sensor **1** could meet the requirement of response time for real time detection in practical samples.

The reversibility of fluorescence response process of sensor **1** to Fe^{3+} was also investigated with ethylenediamine tetraacetic acid disodium salt ($EDTANa_2$). After addition of excess $EDTANa_2$ (30 equiv) to sensor **1** ($1 \cdot 10^{-5}$ M, 1 equiv) and Fe^{3+} (10 equiv) solution, the fluorescence spectrum of the resulted solution restored near to the original spectrum of sensor **1** solution, which indicates that the Fe^{3+} recognition is complex and reversible process.

UV-Vis spectra changes of sensor **1** upon the addition of metal ions further demonstrated the selectivity and sensitivity of sensor **1** to Fe^{3+}. The UV-Vis spectrum of sensor **1** presented a broad absorption band with two peaks at 290 and 398 nm, respectively (Fig. 5*a*). The two absorption peaks were ascribed to the π~π transition of the C=N group and an intermolecular charge transfer (ICT) of the entire conjugated molecule, respectively.[24]

The selectivity of sensor **1** in DMF ($1 \cdot 10^{-5}$ M) was examined with various metal ions (including K^+, Ag^+, Mn^{2+}, Co^{2+}, Ni^{2+}, Zn^{2+}, Cd^{2+}, Mg^{2+}, Ca^{2+}, Sr^{2+}, Ba^{2+}, Hg^{2+}, Fe^{2+}, Cu^{2+}, Al^{3+}, Cr^{3+}, Fe^{3+}, and Pb^{2+} at 10 equiv). As shown in Figure 5*a*, after Fe^{3+} ion coordinated with sensor **1**, the entire absorption band increased significantly. Meanwhile, the color of the solution became deep yellow. The addition of other metal ions did not cause obvious changes of the absorption peaks except for Pb^{2+}, that

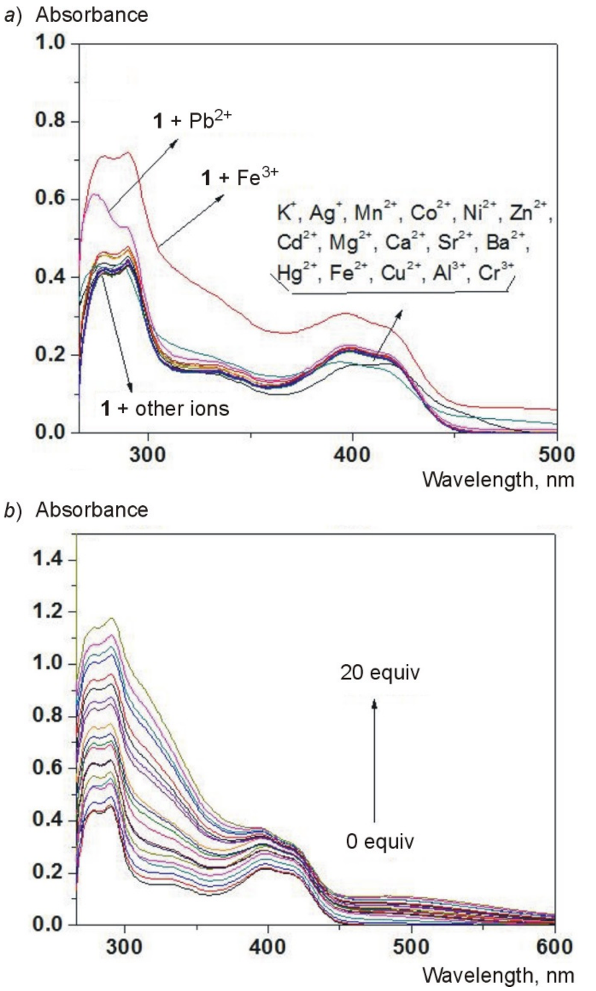

Figure 5. *a*) The changes of UV-Vis spectra of sensor **1** in DMF ($1 \cdot 10^{-5}$ M) upon the addition of different metal ions (10 equiv). *b*) The titration spectra of sensor **1** in DMF ($1.0 \cdot 10^{-5}$ M) with Fe^{3+} (0–20 equiv).

induced the partial absorption band between 260–315 nm increase. The above results are consistent with fluorescence measurements and confirm the high selectivity of fluorescence sensitivity of sensor **1** for Fe^{3+}.

UV-Vis spectrometric titration experiments can help us to study the sensing property of sensor **1** to Fe^{3+}. Therefore, titration of sensor **1** in DMF with Fe^{3+} was subsequently curried out. Upon incremental addition of Fe^{3+} (0–20 equiv) to the sensor **1** solution ($1 \cdot 10^{-5}$ M) resulted in a stepwise increase in absorbance at 290 nm (Fig. 5*b*). This is due to the formation of complexes between sensor **1** and Fe^{3+}, and the absorbance intensity increased gradually with forming of more complexes.

Benesi–Hildebrand plotted from UV-Vis spectra titration is also used to elevate the properties of complexes. Benesi–Hildebrand curve was plotted with $1/(A - A_0)$ as function of $\mathbf{1}/Fe^{3+}$ (Fig. 6). Linear fitting of the experiment plot based on the 1:1 binding stoichiometry of sensor **1** and Fe^{3+} was executed and the fitted curve is almost superimposed over the experimental plot with a correlation coefficient over 0.9881, which supported the result of fluorescence titration and further confirmed the 1:1 binding stoichiometry of sensor **1** with Fe^{3+}. The binding constant between sensor **1** and Fe^{3+} was evaluated to be $1.88 \cdot 10^{-6}$ M^{-1}, which approaches near to the K_a calculated from fluorescence titration.

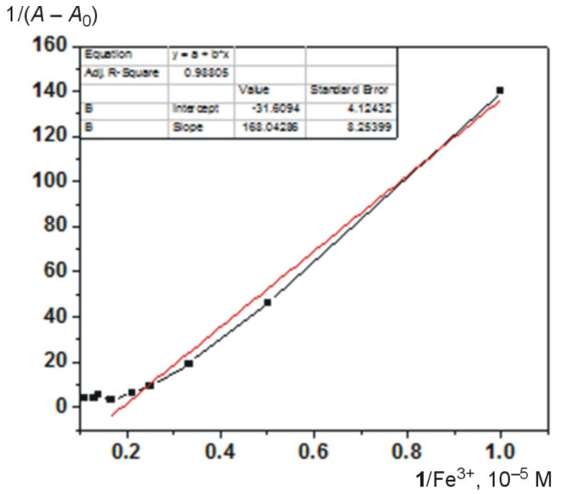

Figure 6. Benesi–Hildebrand plot of sensor **1** in DMF ($1 \cdot 10^{-5}$ M) in the presence of Fe^{3+} (0–10 equiv) (*R* 0.9881).

To investigate the practical application of sensor **1**, we used the calibration curve in Figure 4*b* to determine Fe^{3+} ion concentration in distilled and tap water samples in DMF solution. Each sample was analyzed with three replicates, a suitable recovery and R.S.D. values of the water samples were obtained, as shown in Table 1. These results suggest that sensor **1** could be useful for the measurement of Fe^{3+} in chemical and environmental applications.

The response of the fluorescence and absorbance of sensor **1** to Fe^{3+} evidenced complex formation between sensor **1** and Fe^{3+} with the 1:1 stoichiometry. In the sensor **1** molecule, the nitrogen atoms of C=N group with lone electron pair has strong coordination ability and can coordinate with Fe^{3+} atoms.[22] Based on the above results, we proposed the binding mode (Scheme 2).

In conclusion, the fluorescent chemosensor containing double Schiff base based on the carbazole and diaminomaleonitrile was synthesized. The experimental results of fluorescence and absorbance spectra indicated that sensor has high selectivity and sensitivity toward Fe^{3+} ions. Job's plot and titration experiments demonstrated that sensor formed the 1:1 complex with Fe^{3+}. Sensor presented the large binding constant for Fe^{3+} ($7.98 \cdot 10^{-6}$ M^{-1}) indicating the greater affinity to Fe^{3+} than the other competitive metal ions. Sensor also presented low detection limit ($3.75 \cdot 10^{-8}$ M) and fast fluorescence response to Fe^{3+} (15 s) indicating

Table 1. Determination of Fe^{3+} in water samples*

Sample	Fe^{3+} added, 10^{-5} mol·l^{-1}	Fe^{3+} found, 10^{-5} mol·l^{-1}	Recover, %	R.S.D. (n = 3), %
Distilled water	0.00	0.00		
	4.00**	4.13	103.3	1.9
Tap water	0.00	0.00		
	4.00**	3.90	97.5	2.1

* Conditions: sensor **1** (10 μmol·l^{-1}) in DMF solution.
** $4.00 \cdot 10^{-5}$ mol·l^{-1} of Fe^{3+} ions was artificially added.

Scheme 2. Proposed binding mechanism of sensor **1** with Fe^{3+}

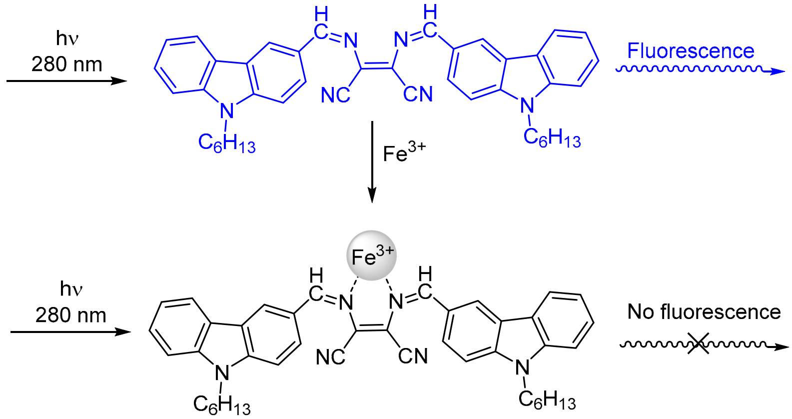

applicability for the real-time detection. These results indicate that the compound has great potential as fluorescent chemosensor for Fe^{3+} detection in real samples.

Experimental

The IR spectra were recorded on a Nicolet 6700 Fourier Transform Infrared Spectrometer in KBr pellets. ^1H and ^{13}C NMR spectra were recorded on a Varian Unity Inova Spectrometer (500 and 125 MHz, respectively) at room temperature in $CDCl_3$ with TMS as internal standard. High-resolution mass spectra recorded on Agilent 1200 HPLC/Micro TOF spectrometer, electrospray ionization. Absorbance and fluorescence spectra were recorded using a Varian Cary 500 UV-Vis spectrophotometer and a Cary Eclipse Fluorescence Spectrophotometer, respectively.

9*H*-Carbazole, 1-bromohexane, $POCl_3$, 2,3-diaminomaleonitrile were purchased from Sinopharm Group Co. Ltd. and used without further purification. The salts used in metal ion stock solutions were $Cu(NO_3)_2·3H_2O$, $Ni(NO_3)_2·6H_2O$, $Al(NO_3)_3·9H_2O$, $Zn(NO_3)_2·6H_2O$, $Cr(NO_3)_3·9H_2O$, $Cd(NO_3)_2·4H_2O$, $Fe(NO_3)_3·9H_2O$, $Co(NO_3)_2·6H_2O$, $Mg(NO_3)_2·6H_2O$, KNO_3, $AgNO_3$, $BaCl_2·2H_2O$, $MnCl_2$, $HgCl_2$, $PbCl_2$, $CaCl_2$, $SrSO_4$, and $FeSO_4·7H_2O$.

9-Hexyl-9*H*-carbazole (3). 9*H*-Carbazole (6.2 g, 37.0 mmol) was added to a solution of KOH (13.0 g, 232.0 mmol) in DMF (85 ml) in a 250-ml flask, and the resulting mixture stirred at room temperature for 40 min. Then 1-bromohexane (5.27 ml, 37.0 mmol) was added dropwise and stirring continued for 9 h. The mixture was poured into cold water and white precipitate was formed. Precipitate was filtered and purified by column chromatography (eluent petroleum ether – CH_2Cl_2, 3:1) to give the desired product. Yield 9.10 g (98%), white powder, mp 62–63°C (mp 62–63°C[38]). ^1H NMR spectrum, δ, ppm (*J*, Hz): 8.10 (2H, d, *J* = 4.0, H Ar); 7.48–7.45 (2H, m, H Ar); 7.40 (2H, d, *J* = 4.0, H Ar); 7.25–7.21 (2H, m, H Ar); 4.30 (2H, t, *J* = 7.5, CH_2); 1.90–1.84 (2H, m, CH_2); 1.40 (2H, t, *J* = 6.25, CH_2); 1.38–1.25 (4H, m, CH_2); 0.86 (3H, t, *J* = 7.0, CH_3).

9-Hexyl-9*H*-carbazole-3-carbaldehyde (2). A solution of $POCl_3$ (9.1 ml, 100.0 mmol) in DMF (81.0 ml, 100.0 mmol) was stirred on an ice-water bath for 40 min, the solution was warmed up to room temperature and stirred for additional 1 h. Then a solution of 9-hexyl-9*H*-carbazole (**3**) (2.51 g, 10.0 mmol) in 1,2-dichloroethane (50 ml) was added dropwise, and the reaction mixture was refluxed for 24 h. After cooling to room temperature, the mixture was poured into ice water, neutralized with 50% NaOH aqueous solution and then extracted with CH_2Cl_2 (4×50 ml). The combined organic phase was sequentially washed with saturated $NaHCO_3$ solution and saturated NaCl solution, then dried over anhydrous Na_2SO_4. The solvent was evaporated under reduced pressure, and the crude product was purified by column chromatography (eluent petroleum ether – EtOAc, 3:1). Yield 4.17 g (75%), white powder, mp 63–64°C (mp 63–64°C[39]). ^1H NMR spectrum, δ, ppm (*J*, Hz): 10.10 (1H, s, CHO); 8.61 (1H, d, *J* = 0.5, H Ar); 8.16 (1H, d, *J* = 3.8, H Ar); 8.02–8.00 (1H, m, H Ar); 7.55–7.52 (1H, m, H Ar); 7.47 (2H, t, *J* = 8.3, H Ar); 7.34–7.31 (1H, m, H Ar); 4.33 (2H, t, *J* = 7.3, CH_2); 1.92–1.86 (2H, m, CH_2); 1.41–1.35 (2H, m, CH_2); 1.34–1.26 (4H, m, CH_2); 0.86 (3H, t, *J* = 7.3, CH_3).

2,3-Bis[(9-Hexyl-9*H*-carbazol-3-yl)methylideneamino]-maleonitrile (1). A mixture of 2, 3-diaminomaleonitrile (0.27 g, 2.5 mmol), 9-hexyl-9*H*-carbazole-3-carbaldehyde (**2**) (1.53 g, 5.5 mmol) in EtOH (30 ml) in a 100-ml flask was stirred at 70°C for 7 h. The solvent was distilled off, and residue was purified by column chromatography (petroleum ether – CH_2Cl_2, 3:1). Yield 0.15 g (10%), orange powder, mp 169–171°C. IR spectrum, ν, cm^{-1}: 3808, 3436, 2923, 2855, 2209, 1583, 1469, 1381, 1240, 1196, 1125, 807, 743, 616, 565, 438, 408. ^1H NMR spectrum, δ, ppm (*J*, Hz): 8.97 (2H, s, HC=N); 8.68 (2H, s, H Ar); 8.14 (2H, d, *J* = 4.0, H Ar); 7.56–7.45 (8H, m, H Ar); 7.35 (2H, t, *J* = 9.0, H Ar); 4.35 (4H, t, *J* = 8.8, NCH_2); 1.91 (4H, t, *J* = 9.3, CH_2); 1.40 (4H, d, *J* = 9.5, CH_2); 1.32 (8H, s, CH_2); 0.88 (6H, t, *J* = 8.8, CH_3). ^{13}C NMR spectrum, δ, ppm: 164.8; 143.8; 141.0; 131.0; 127.8; 126.7; 126.2; 125.8; 124.4; 123.5; 122.9; 120.9; 120.4; 111.5; 110.5; 109.5; 109.4; 43.5; 31.5; 28.9; 26.9; 22.5; 14.0. Found, *m/z*: 655.3741 [M+Na]. $C_{42}H_{42}N_6$. Calculated, *m/z*: 655.3769.

Selectivity experiments. Both absorbance and fluorescence spectra were used to investigate the selective response of sensor **1** to metal ions. Sensor **1** (3.15 mg, 0.005 mmol) was dissolved in DMF (20 ml) and then transferred into 500-ml volumetric flask. After the DMF was added to the volumetric scale mark, the $1·10^{-5}$ M solution of sensor **1** was obtained. $Cu(NO_3)_2 \cdot 3H_2O$, $Ni(NO_3)_2 \cdot 6H_2O$, $Al(NO_3)_3 \cdot 9H_2O$, $Zn(NO_3)_2 \cdot 6H_2O$, $Cr(NO_3)_3 \cdot 9H_2O$, $Cd(NO_3)_2 \cdot 4H_2O$, $Fe(NO_3)_3 \cdot 9H_2O$, $Co(NO_3)_2 \cdot 6H_2O$, $Mg(NO_3)_2 \cdot 6H_2O$, KNO_3, $AgNO_3$, $BaCl_2 \cdot 2H_2O$, $MnCl_2$, $HgCl_2$, $PbCl_2$, $FeSO_4 \cdot 7H_2O$, $CaCl_2$, and $SrSO_4$ (0.25 mmol) were dissolved in deionized H_2O (50 ml) to make $5 \cdot 10^{-3}$ M metal ion solutions, respectively.

For selectivity test, a series of mixed solutions of sensor **1** and different metal ions were prepared. The each test solution was prepared by placing 0.05 ml of the metal ion solution ($5 \cdot 10^{-3}$ M, 10 equiv) in 2.5 ml sensor **1** solution ($1 \cdot 10^{-5}$ M, 1 equiv), respectively. After mixing them for 3 min, UV-Vis absorbance and fluorescence spectra were recorded at room temperature.

Absorbance and fluorescence titration. Fe^{3+} stock solution was diluted to different required concentration ($1 \cdot 10^{-3}$ – $0.5 \cdot 10^{-3}$ M) in H_2O. For each titration, solution with different molar ratio of Fe^{3+} to sensor **1** was prepared by adding 50 μl of diluted Fe^{3+} solution to 2.5 ml solution of sensor **1** ($1 \cdot 10^{-5}$ M). The concentration of sensor **1** in every solution was kept at $1 \cdot 10^{-5}$ M. The absorbance and fluorescence spectra were recorded at room temperature after mixing the test solution for 3 min. In titration experiment, the volume of Fe^{3+} solution added into sensor **1** solution did not exceed 2% of sensor **1** volume in case that the concentration of sensor **1** was obviously influenced.

Job's plot measurements. The stoichiometry of complex can be estimated by Job's plot *via* the measurement of absorbance and fluorescence spectra. Job's plot was drawn based on the measurement of a series of solutions in which the molar concentrations of metal ion and ligand vary, but their sum remains constant. The absorbance or fluorescence of each solution was measured and the Job's plot was obtained by plotting the maximum value of absorbance or fluorescence against the mole fraction of metal ion or ligand. The maximum or the inflection point on the Job's plot appear at the mole ratio corresponding to the combining ratio of the complex.

Supplementary information file containing ^1H and ^{13}C NMR, MS, emission, fluorescence and spectrophotometric titration spectra of compound **1** is available at the journal website at http://link.springer.com/journal/10593.

This work was supported by the Research Fund for the Doctoral Program of Higher Education of China (20120043110007).

References

1. Carter, K. P.; Young, A. M.; Palmer, A. E. *Chem. Rev.* **2014**, *114*, 4564.
2. Li, H.; Fan, J.; Peng, X. *Chem. Soc. Rev.* **2013**, *42*, 7943.
3. Dai, H. L.; Yan, Y. Y.; Guo, Y.; Fan, L. L.; Che, Z. P.; Xu, H. *Chem.–Eur. J.* **2012**, *18*, 11188.
4. Georgopoulos, P. G.; Roy, A.; Yonone-Lioy, M. J.; Opiekun, R. E.; Lioy, P. J. *J. Toxicol. Environ. Health*, *Part B* **2001**, *4*, 341.
5. Wang, Y.; Chang, H.-Q.; Wu, W.-N.; Zhao, X.-L.; Yang, Y.; Xu, Z.-Q.; Xu, Z.-H.; Jia, L. *Sens. Actuators*, *B* **2017**, *239*, 60.
6. Frausto da Silva, J. J. R.; Williams, R. J. P. *The Biological Chemistry of the Elements: The Inorganic Chemistry of Life*; Oxford Universuty Press: New York, 1991, p. 344.
7. Burdo, J. R.; Connor, J. R. *BioMetals* **2003**, *16*, 63.
8. Minkin, V. I.; Bren', V. A.; Dubonosov, V. A.; Tsukanov, A. V. *Chem. Heterocycl. Compd.* **2012**, *48*, 107. [*Khim. Geterotsikl. Soedin.* **2012**, 112.]
9. Pan, J.-T.; Zhu, F.; Kong, L.; Yang, L.-M.; Tao, X.-T.; Tian, Y.-P.; Lu, H.-B.; Yang, J.-X. *Chem. Pap.* **2015**, *69*, 527.
10. Wu, H.-L.; Aderinto, S. O.; Xu, Y.-L.; Zhang, H.; Fan, X.-Y. *J. Appl. Spectrosc.* **2017**, *84*, 25.
11. Tolpygin, I. E.; Tihomirova, K. S.; Popova, O. S.; Nikolaeva, O. G.; Revinskii, Yu. V.; Dubonosov, A. D.; Bren, V. A. *Chem. Heterocycl. Compd.* **2014**, *50*, 41. [*Khim. Geterotsikl. Soedin.* **2014**, 47.]
12. Tikhomirova, K. S.; Tolpygin, I. E.; Starikov, A. G.; Kaz'mina, M. A. *Chem. Heterocycl. Compd.* **2017**, *53*, 179. [*Khim. Geterotsikl. Soedin.* **2017**, *53*, 179.]
13. Wang, C.; Zhou, J. D.; Ran, G. X.; Li, F.; Zhong, Z.; Song, Q. J.; Dong, Q. C. *J. Mater. Chem. C* **2017**, *5*, 434.
14. Chai, M. M.; Li, M.; Zhang, D.; Wang, C.-C.; Ye, Y.; Zhao, Y. F. *Luminescence* **2013**, *28*, 557.
15. Zhang, Y. Q.; Wang, G.; Zhang, J. P. *Sens. Actuators*, *B* **2014**, *200*, 259.
16. Zhao, B.; Liu, T.; Fang, Y.; Wang, L.Y.; Kan, W.; Deng, Q. G.; Song, B. *Sens. Actuators*, *B* **2017**, 246, 370.
17. Tang, L. J.; Wu, D.; Hou, S. H.; Wen, X.; Dai, X. *Bull. Korean Chem. Soc.* **2014**, *35*, 2326.
18. Li, D. X.; Sun, X.; Huang, J. M.; Wang, Q.; Feng, Y.; Chen, M.; Meng, X.; Zhu, M.; Wang, X. *Dyes. Pigm.* **2016**, *125*, 185.
19. Yang, L. L.; Wang, J. P.; Yang, L.; Zhang, C.; Zhang, R. L.; Zhang, Z. P.; Liu, B. H.; Jiang, C. L. *RSC. Adv.* **2016**, *6*, 56384.
20. Gündüz, Z. Y.; Gündüz, C.; Özpinar, C.; Urucu, O. A. *Spectrochim. Acta*, *Part A* **2015**, *136*, 1679.
21. Cao, B.-N.; Hu, Q.; Huang, Y.; Jia, C.-M.; Zhang, Q. *Chem. Res. Chin. Univ.* **2013**, *29*, 419.
22. Mergu, N.; Gupta, V. K. *Sens. Actuators*, *B* **2014**, *210*, 408.
23. Vikneswaran, R.; Syafiq, M. S.; Eltayeb, N. E.; Kamaruddin, M. N.; Ramesh, S.; Yahya, R. *Spectrochim. Acta*, *Part A* **2015**, *150*, 175.
24. Yang, L. L.; Zhu, W. J.; Fang, M.; Zhang, Q.; Li, C. *Spectrochim. Acta*, *Part A* **2013**, *109*, 186.
25. Zakrzewska, A.; Zalesny, R.; Kolehmainen, E.; Osmia1owski, B.; Jedrzejewska, B.; Agren, H.; Pietrzak, M. *Dyes Pigm.* **2013**, *99*, 957.
26. Osmialowski, B.; Zakrzewska, A.; Jedrzejewska, B.; Grabarz, A.; Zalesny, R.; Bartkowiak, W.; Kolehmainen, E. *J. Org. Chem.* **2015**, *80*, 2072.
27. Zhao, B.; Liu, T.; Fang, Y.; Wang, L. Y.; Kan, W.; Deng, Q. G.; Song, B. *Sens. Actuators*, *B* **2017**, *246*, 370.
28. Wu, J.-S.; Liu, W.-M.; Zhuang, X.-Q.; Wang, F.; Wang, P.-F.; Tao, S.-L.; Zhang, X.-H.; Wu, S.-K.; Lee, S.-T. *Org. Lett.* **2006**, *9*, 33.
29. Ghosh, K.; Rathi, S.; Rathi, P.; Gupta, P.; Vashisth, P.; Pruthi, V. *Eur. J. Inorg. Chem.* **2015**, 311.
30. Goswami, S.; Das, S.; Aich, K. *Tetrahedron Lett.* **2013**, *54*, 4620.
31. Schaming, D.; Costa-Coquelard, C.; Lampre, I.; Sorgues, S.; Erard, M.; Liu, X.; Liu, J.; Sun, L.; Canny, J.; Thouvenot, R.; Ruhlmann, L. *Inorg. Chim. Acta* **2010**, *363*, 2185.
32. Hibbert, D. B.; Thordarson, P. *Chem. Commun.* **2016**, *52*, 12792.
33. Liu, S.-R.; Wu, S.-P. *J. Fluoresc.* **2011**, *21*, 1599.
34. Yi, C.; Tian, W.; Song, B.; Zheng, Y.; Qi, Z.; Qi, Q.; Sun, Y. *J. Lumin.* **2013**, *141*, 15.
35. Yin, J.; Bing, Q. J.; Wang, L.; Wang, G. *Spectrochim. Acta*, *Part A* **2018**, *189*, 495.
36. Chen, H. L.; Bao, X. F.; Shu, H.; Zhou, B. J.; Ye, R. L.; Zhu, J. *Sens. Actuators*, *B* **2017**, *242*, 921.
37. Liu, J. W.; Lu, Y. *J. Am. Chem. Soc.* **2007**, *129*, 9838.
38. Hwang, S.-H.; Wang, P.; Moorefield, C. N.; Godinez, L. A.; Manriquez, J.; Bustos, E.; Newkome, G. R. *Chem. Commun.* **2005**, 4672.
39. Grigoras, M.; Antonoaia, N.-C. *Eur. Polym. J.* **2005**, *41*, 1079.